HHS Public Access
Author manuscript
Kidney Int. Author manuscript; available in PMC 2017 March 01.

Published in final edited form as:
Kidney Int. 2016 March ; 89(3): 565–573. doi:10.1016/j.kint.2015.12.020.

Increased bone density in mice lacking the proton receptor, OGR1

Nancy S. Krieger[1], **Zhenqiang Yao**[2], **Kelly Kyker-Snowman**[1], **Min Ho Kim**[1], **Brendan F. Boyce**[2], and **David A. Bushinsky**[1]

[1]Department of Medicine, University of Rochester School of Medicine and Dentistry, Rochester, NY 14642

[2]Department of Pathology, University of Rochester School of Medicine and Dentistry, Rochester, NY 14642

Abstract

Chronic metabolic acidosis stimulates cell-mediated calcium efflux from bone through osteoblastic prostaglandin E2-induced stimulation of RANKL leading to increased osteoclastic bone resorption. Osteoblasts express the proton-sensing G-protein coupled receptor, OGR1, which activates IP3-mediated intracellular calcium. Proton-induced osteoblastic intracellular calcium signaling requires OGR1, suggesting OGR1 is the sensor activated during acidosis to cause bone resorption. Growing mice produce large amounts of metabolic acids which must be buffered, primarily by bone, prior to excretion by the kidney. Here we tested whether lack of OGR1 inhibits proton-induced bone resorption by measuring bone mineral density by μCT and histomorphometry in 8 week old male OGR1−/− and C57/Bl6 wild type mice. OGR1−/− mice have normal skeletal development with no atypical gross phenotype. Trabecular and cortical bone volume was increased in tibiae and vertebrae from OGR1−/−. There were increased osteoblast numbers on the cortical and trabecular surfaces of tibiae from OGR1−/− mice, increased endocortical and trabecular bone formation rates, and osteoblastic gene expression. Osteoclast numbers and surface were increased in tibiae of OGR1−/− mice. Thus, in rapidly growing mice, lack of OGR1 leads to increased bone mass with increased bone turnover and a greater increase in bone formation than resorption. This supports the important role of the proton receptor, OGR1, in the response of bone to protons.

Keywords

metabolic acidosis; proton; OGR1; bone resorption; bone formation

---

Corresponding author: Nancy S. Krieger, Ph.D., Division of Nephrology, Dept. Medicine – Box 675, University of Rochester School of Medicine, 601 Elmwood Ave., Rochester, NY 14642, Nancy_Krieger@urmc.rochester.edu, phone: 585-275-5123, fax: 585-442-9201.

Disclosure

The authors have nothing to disclose.

Publisher's Disclaimer: This is a PDF file of an unedited manuscript that has been accepted for publication. As a service to our customers we are providing this early version of the manuscript. The manuscript will undergo copyediting, typesetting, and review of the resulting proof before it is published in its final citable form. Please note that during the production process errors may be discovered which could affect the content, and all legal disclaimers that apply to the journal pertain.

Introduction

Chronic metabolic acidosis (MET), a systemic increase in proton (H^+) concentration due to a reduction in bicarbonate (HCO_3^-) concentration is present during a number of clinical disorders, such as chronic kidney disease and renal tubular acidosis (1). MET induces a direct loss of calcium (Ca) from bone in the process of buffering the acid load (1–3). Using an in vitro model of MET, we found that in the first few hours this loss of Ca from bone occurs through physicochemical mineral dissolution (4, 5) and subsequently by cell-mediated bone resorption (4, 6–8). We have shown previously that MET regulates specific gene expression in osteoblasts, decreases collagen synthesis and subsequent mineralization, and promotes osteoclastic bone resorption (8–11). Acid-induced bone resorption is mediated primarily by stimulation of osteoblastic cyclooxygenase 2 (COX2) leading to a prostaglandin E_2-mediated increase in RANKL expression (12–14). RANKL interacts with its receptor, RANK, on osteoclast precursors, leading to differentiation and activation of osteoclasts, increased bone resorption and subsequent net Ca efflux from bone (15).

We and others have demonstrated that osteoblasts express the G protein-coupled H^+ sensing receptor, OGR1 (16,17,18). This receptor senses extracellular H^+ through histidine residues and is coupled to G_q, stimulating inositol phosphate (IP_3) production and mobilization of intracellular Ca (Ca_i) (17, 19). OGR1 is expressed in osteoblasts and osteocytes as well as osteoclasts, and has been found in other tissues and neoplastic cells (19). We found that H^+ activation of OGR1 results in increased Ca_i signaling in osteoblasts and that the OGR1 inhibitor, $CuCl_2$, which directly stabilizes histidine residues in OGR1, inhibits H^+-induced stimulation of bone resorption in cultured neonatal mouse calvariae {(16)}. Pharmacologic inhibition of IP_3-mediated Ca_i release also inhibits H^+-induced intracellular signaling in osteoblasts and bone resorption (20). Our findings strongly suggest that OGR1 is the H^+ sensor that detects the increase in $[H^+]$ during metabolic acidosis and initiates osteoblastic signaling leading to increased osteoclastic bone resorption.

Mammalian basal metabolic rate is inversely correlated with mammalian body size, being highest in the smallest animals (21). Endogenous metabolic acids must be buffered, in large part by bone (6, 22), prior to renal excretion (1, 3). Since our prior work indicated that OGR1 is the H^+ sensor which initiates the bone response to metabolic acidosis, we hypothesized that the lack of OGR1 would protect the skeleton from acid-induced bone resorption in rapidly growing mice. To test the hypothesis that the lack of OGR1 would inhibit H^+-induced bone resorption, we determined bone mineral density and bone histomorphometric parameters of mice with a genetic null mutation in OGR1 (OGR1−/−) compared to wild type mice. In OGR1−/− mice the observation of increased bone mineral density, with increased bone formation and decreased bone resorption, would support this hypothesis.

Results

Gross Phenotype

At 8 weeks of age there is no gross phenotypic or size difference between male OGR1−/− and WT mice and no significant difference in body weight (OGR1−/− = 22.8±0.6 vs. WT = 23.8±0.2 gm).

Immunohistochemistry

To confirm the absence of OGR1 in bones from OGR1−/− mice, tibial sections were stained with a specific OGR1 antibody. Immunohistochemical analysis did not demonstrate staining in the absence of the primary antibody (Fig. 1, panel A), positive staining in osteoblasts on bone surfaces in tibial sections from WT (Fig. 1, panel B) and the absence of specific OGR1 staining in OGR1−/− bone (Fig. 1, panel C). Immunoblot analysis of total protein from primary calvarial cells demonstrates OGR1 in cell lysates from wild type but not from OGR1 −/− mice (Fig. 1D).

Micro-computed Tomography (μCT)

Tibiae and vertebrae from OGR1−/− and WT mice were analyzed by μCT. Representative images of tibiae show increased trabecular bone density in the OGR1−/− mice compared to WT mice (Fig. 2A). Quantitative analysis of μCT images demonstrate significantly increased trabecular bone volume/total volume and increased trabecular number and decreased trabecular spacing in the OGR1−/− tibiae (Fig. 2B). Representative μCT images of vertebrae also demonstrate increased trabecular bone density in the OGR1−/− vertebrae (Fig. 3A). Quantitative analysis of μCT images demonstrates significantly increased trabecular bone volume/total volume, increased trabecular number and thickness and decreased trabecular spacing in the OGR1−/− vertebrae (Fig. 3B). Tibial cortical bone volume is increased in the OGR1−/− mice, as illustrated in representative μCT images (Fig. 4A). Quantitative analysis of the μCT of tibial cortical bone demonstrates significantly increased cortical bone area as well as increased cortical thickness from OGR1−/− mice (Fig. 4B).

Osteoblast Histomorphometry and Bone Formation Rate

Representative H&E-stained sections of tibiae from WT (upper panels) and OGR1−/− (lower panels) mice demonstrate that OGR1−/− mice have increased trabecular bone volume (Fig. 5A). Histomorphometric analysis of these sections demonstrates an increase in % bone volume and a decrease in trabecular spacing (Fig. 5B), which is similar to the results obtained with μCT (Fig. 2 and Fig. 4). By histomorphometric analysis there was an increase in osteoblast number along the endocortical and trabecular bone surface of OGR1−/− tibia (Fig. 6A). Bone formation rates, as determined by in vivo calcein labeling, were also significantly increased in both endocortical and trabecular bone in OGR1−/− tibiae (Fig. 6B).

Osteoblastic Gene Expression

To further define the role of the osteoblast in the increased density of bones from OGR1−/− mice we isolated primary osteoblasts from OGR1−/− and wild type neonatal calvariae and examined characteristic osteoblast gene expression levels in these cells. When grown to confluence (0′), we found significantly greater expression of alkaline phosphatase, collagen 1, osterix, runx2 and RANKL in the knockout osteoblasts compared to wild type (Fig. 7A). When these cultures were switched to mineralization medium and allowed to further differentiate for an additional 2 weeks, expression of these same osteoblast genes remained higher in the knockout than in the wild type osteoblasts. There was no difference in the level of osteocalcin expression at either time point (Fig. 7B). Additional cultures were stained with alizarin red after 2 weeks in mineralization medium to determine the extent of mineralization. There was significantly more staining in the OGR1−/− cultures compared to wild type cultures (Fig. 7C).

Osteoclasts

Histomorphometric analysis of H&E stained sections demonstrate an increase in osteoclast number and osteoclast surface in the tibial metaphyses of OGR1−/− mice compared to wild type (Fig. 8A). There is also an increase in tartrate resistant acid phosphatase staining in OGR1−/− mice compared to wild type (Fig. 8B).

Discussion

Rapidly growing mice generate large amounts of metabolic acids (21) which must be buffered, principally by bone, before they are ultimately excreted by the kidney. We have shown previously that MET directly regulates both osteoblastic and osteoclastic activity (8, 23), decreases collagen synthesis and mineralization and increases osteoclastic bone resorption (8, 11), responses which are mediated by H^+ signaling in the osteoblast through the H^+ receptor OGR1 (16, 20). OGR1 is a H^+-sensing receptor that stimulates inositol phosphate formation and increases Ca_i and is found in osteoblasts, osteocytes and chondrocytes (17, 19), as well as other tissues (19, 24). We previously confirmed the expression of OGR1 in mouse osteoblasts and found that inhibition of OGR1 with $CuCl_2$ decreased acid-induced bone resorption (16). MET increased Ca_i in CHO cells stably transfected with OGR1 comparably to the H^+-induced increases in Ca_i observed in primary mouse osteoblasts (16). In contrast, non-transfected CHO cells did not increase Ca_i in response to MET. Further support for OGR1 mediating the response to H^+ in osteoblasts is our finding that pharmacologic inhibition of increased Ca_i blocks acid-induced stimulation of COX2 and RANKL in primary osteoblasts, as well as H^+-induced osteoclastic bone resorption (20).

To further test the hypothesis that OGR1 is important in the osseous response to acid we determined the bone mineral density and histomorphometry of mice with a genetic null mutation in OGR1 (OGR1−/−) compared to age and sex matched WT mice. We found that male mice lacking OGR1 have increased bone density and increased bone formation compared to WT controls. However in addition to the increase in bone formation rate we found an increased number of osteoclasts and increased TRAP staining in the OGR1−/−

mice, suggesting increased bone resorption. In 8 week old growing mice, there is active bone remodeling, with ongoing bone formation and bone resorption. Given the observed increased bone density in OGR1−/− mice, the measured increase in bone formation must exceed any increase in bone resorption. Although the increased expression of osteoblastic genes would contribute to the increase in bone formation, the increase in RANKL gene expression should contribute to the increased resorption. Further studies will be necessary to directly characterize the activity of osteoclasts isolated from these mice. The current findings support our hypothesis that OGR1 is an important H^+ sensor in bone which detects the increase in H^+ concentration and initiates the signal transduction cascade leading to MET-induced, increased cell-mediated bone resorption and decreased bone formation. While the results of this study are consistent with decreased proton sensing in the OGR1−/− mice, this interpretation is limited by our inability to directly measure arterial blood pH in these mice. Future studies may require direct measurement of arterial blood gases in unanesthetized and unstimulated mice.

That OGR1 is a primary mediator of the response by osteoblasts to increased $[H^+]$ is consistent with our current findings that both trabecular and endocortical bone formation rates were significantly increased in OGR1−/− tibiae. In this study μCT analyses demonstrated that vertebral and tibial trabecular bone volume and trabecular number were increased and trabecular spacing was decreased in OGR1−/− mice; vertebral trabecular thickness and tibia cortical bone volume were also increased in OGR1−/− compared to WT bones. Histomorphometric analyses of tibia sections also demonstrated an increase in trabecular bone volume. In contrast to the increased bone formation in OGR1−/− mice, metabolic acidosis decreases collagen synthesis in calvariae from mice with intact OGR1 (8). Supporting the current observations, Tomura et al. found that in human osteoblastic cells an acidic pH induced a transient increase in Ca_i and inositol phosphate production as well as increased COX2-mediated PGE_2 production (18). Inhibition by siRNA for OGR1 blocked these responses, again supporting the primary role for OGR1 as the osteoblastic signal transducer for H^+ in bone.

In addition to being the H^+ sensor in osteoblasts, OGR1 appears to have a direct role in the response of osteoclasts to acid. As with RANKL-induced activation of osteoclasts (15, 25), metabolic acidosis directly activated isolated osteoclasts by a Ca_i-mediated stimulation of NFATc1 (26). Osteoclasts also express OGR1, which increased in response to RANKL treatment (26). Proton-induced increases in Ca_i in osteoclasts were blocked by zinc, presumably due to inhibition of OGR1 (26). Both CSF-1 and RANKL stimulated OGR1 expression and osteoclast differentiation in vivo and also in vitro in isolated pre-osteoclasts (RAW 264.7 cells) (27). Acidosis increased the survival of isolated osteoclasts, possibly by suppressing apoptosis, and survival was lessened by depleting OGR1 using RNA interference (28). Li et al. generated a conditional OGR1-deficient mouse by homologous recombination (29). They found no gross abnormalities in bones of these knockout mice by X-ray or histomorphometry. However, using isolated bone marrow cells from these mice, they observed fewer osteoclasts in response to M-CSF and RANKL induction. In contrast to the findings of Pereverzev, Li found that osteoclasts from knockout mice had a similar survival rate at pH 7.4 and pH 6.8, while osteoclasts from wild type mice had reduced survival at the lower pH. Thus, OGR1 appears to play a direct role in osteoclast differentiation and function in addition to its role in osteoblast activation by H^+.

It is unclear why there is an increase in RANKL and osteoclast activity in addition to an increase in osteoblastic bone formation in the OGR1−/− mice. However, a simultaneous increase in both bone resorption and bone formation is not unique to OGR1−/− mice. For example constant, excessive PTH, such as found in primary hyperparathyroidism results in both an increase in bone formation and bone resorption with resorption predominating over formation, resulting in a decrease in bone mass (30). In contrast small intermittent exogenous doses of PTH result in increased bone formation and increased bone mass (30). Future studies of osteoclast regulation in OGR1−/− mice will be needed to understand the role of this cell in the increase in bone mass of this animal.

In this study, while we found an increase in osteoclast number in OGR1−/− mice, there was also an increase in the osteoblast number and bone formation rate. In addition, primary osteoblasts from OGR1−/− calvariae demonstrated increased expression of genes characteristic of differentiated osteoblasts. The net increase in trabecular and cortical bone mass in the OGR1−/− mice therefore almost certainly represents a net increase in bone formation relative to bone resorption. Although there is an overall increase in bone remodeling in the OGR1−/− mice, the data support an imbalance in favor of increased bone formation. In this study OGR1 was absent in both osteoblasts and osteoclasts. While the increase in osteoblastic bone formation must be due to the lack of OGR1 in the osteoblast, we cannot yet determine if the increase in osteoclast number was due to a lack of osteoclastic OGR1 or mediated through the osteoblast. This determination will require generation of a conditional deletion of OGR1 in osteoblastic and osteoclastic cells and further characterization of the effect of H^+ on isolated osteoblasts and osteoclasts from OGR1−/− mice.

As our model is a global knockout of OGR1, we cannot rule out that the effects we observe are due to a response to OGR1 in other tissues. OGR1 has also been shown to be an active H^+ receptor in non-osseous cells, including human aortic smooth muscle cells (31) which respond to acidic extracellular pH with increased inositol phosphate production, transient increased Ca_i and increased prostaglandin I_2. These responses were blocked when cells were transfected with siRNA specific for OGR1. In addition, OGR1 has been shown to function as a tumor metastasis suppressor gene when overexpressed in human prostate cancer cells in vivo (32). OGR1 is not the only metabolically active H^+ receptor. GPR4 is another G-protein coupled proton receptor that is abundant in the kidney. GPR4−/− mice have decreased net acid excretion resulting in metabolic acidosis (33). OGR1 is of low abundance in the kidney; and would not be expected to play a role in how the kidney detects changes in $[H^+]$, though this has not been tested directly.

In the current study we tested the hypothesis that the lack of OGR1 would inhibit H^+-induced bone resorption in rapidly growing mice that generate large amounts of metabolic acid. We found that mice lacking this H^+ receptor have a net increase in bone formation resulting in increased bone mineral density, supporting this hypothesis. A greater understanding of the importance of OGR1 in the response of bone to excess H^+ may provide new approaches for mitigating the bone loss associated with isolated chronic metabolic acidosis and in metabolic acidosis as part of chronic kidney disease-mineral bone disorder.

Methods

Animals

Mice with a genetic null mutation in OGR1 (OGR1−/−) were provided by K. Seuwen, Novartis (Basel, Switzerland). As OGR1−/− mice were generated on a C57/Bl6 background, wild type C57/Bl6 (WT) mice were used as controls. Eight week old OGR1−/− and WT male mice were used for all comparisons. Bones from at least 12 animals of each genotype were analyzed for histology and for microCT, though not all bones were suitable for use for each analysis. For each determination the number of bones analyzed is listed in the figure legend. When measuring bone formation rate, at 14 days and 2 days prior to sacrifice, mice were injected with 0.6% calcein (Sigma) in buffered saline at pH 7.4. All mice were anesthetized with nembutol and killed by cervical dislocation; intact knee joints (distal femur and proximal tibiae) and lumbar columns were dissected. All procedures were approved by the University Committee for Animal Resources.

Immunohistochemistry

Intact left knee joints were fixed in neutral buffered formalin for 72 hrs, washed and decalcified in 5% formic acid (Immunocal, Decal Chemical Corp) and then paraffin embedded, and sectioned. Sections were baked overnight at 60°C, deparaffinized and rehydrated through graded ethanol solutions. For immunohistochemical analyses, antigen retrieval was performed in 10% hyaluronidase (MP Biomedicals) in PBS for 10 min at 37°C. Endogenous peroxidase was quenched with DAKO Dual Endogenous Enzyme Blocking Reagent for 30 min (Dako). Sections were blocked with normal goat serum (Vectastain Elite Rabbit IgG Kit) for 30 min, and incubated overnight at 4°C with a specific primary OGR1 antibody (LifeSpan BioSciences, Inc.) 1:200 in 2% normal goat serum. Binding was detected with a biotinylated goat anti-rabbit (Vectastain Elite Rabbit IgG Kit) secondary antibody and subsequent incubation with Vectastain ABC Reagent. The color reaction was detected with Vector Impact DAB (Vector SK-4105) and counterstained with hematoxylin (Zymed).

Micro-computed tomography (μCT)

To determine cortical and trabecular bone volume, right tibiae and L2 vertebrae were placed in 70% ethanol and scanned by μCT using a Scanco Medical vivaCT 40 with a resolution of 10.5 micron isotropic (cubical) pixels. Two-dimensional images were used to generate three-dimensional reconstructions and calculate morphometric parameters defining cortical bone and trabecular bone mass and micro-architecture. These include bone volume/tissue volume (BV/TV), trabecular thickness (Tb.Th), trabecular number (Tb.N), trabecular separation (Tb.Sp), cortical bone area and mean bone mineral density.

Histomorphometry

Intact left knee joints were fixed in neutral buffered formalin for 72 hours, washed and decalcified in 10% EDTA, embedded in paraffin, and 3 mm sections were cut from the centers of the tibiae. Hematoxylin and eosin (H&E) and tartrate-resistant acid phosphatase (TRAP) staining were performed using standard protocols. Histomorphometric analysis of a defined region 120 μm below the growth plate, 1400 μm long covering the width of the section inside the cortical bone in the tibial diaphysis was analyzed for % bone volume, trabecular number and spacing as well as osteoclast numbers and surfaces and eroded surfaces and quantified using Visiomorph software (Visiopharm) with an algorithm developed to automatically measure these parameters, according to standard bone histomorphometric practice. Osteoclast number and activity were evaluated from paraffin-embedded tibial sections stained for TRAP activity on the bone surface. Slides were scanned and digitized using an Olympus VS110 whole slide imaging system and then analyzed with Visiopharm image analysis software. For analysis of trabecular osteoblast number, cancellous bone from paraffin-embedded tibial sections was imaged at 20x in the proximal diaphysis beginning 450 μm below the growth plate and extending down 600 μm. An algorithm was developed to automatically measure trabecular bone surface and volume in the two regions using Visiopharm software. Results were normalized as percent osteoblast surface/bone surface. Osteoblast number on the endocortical surface was determined in paraffin-embedded tibial sections using an area calculating algorithm in OsteoMeasure software (Osteometrics, Decatur, GA). Individual osteoblasts were counted in a defined area of each section, the perimeter of outlined regions was quantified, and osteoblast number was normalized to the numbers of pixels for each section.

Bone Formation Rate

After μCT, bones were embedded in plastic (LR White, Polyscience) to determine bone formation rate based on calcein labeling. For trabecular bone, the region of interest examined was 700 μm wide × 550 μm high, centered between cortical bone and 120 μm below the growth plate of each section. For cortical bone the endosteal region of interest was 3 mm below the growth plate for a distance of 550 μm for each section. Bone formation rate (BFR, = MAR x MS/TS) was calculated using the Visiomorph program (Visiopharm) for measurement of total trabecular or cortical surface area (TS), double- (DL) and single-labeled (SL) trabecular or cortical surface to calculate mineralizing surface (MS = DL + ½ SL) and inter-label distance, averaged over measurements every 25 μm, to calculate the mineral apposition rate (MAR).

Primary Bone Cell Culture

Primary bone cells, almost exclusively osteoblasts, were isolated from neonatal OGR1−/− and wild type mouse calvariae by sequential collagenase digestion as described previously (34). After each digestion, released cells were collected and resuspended in the HEPES buffer with 1 mM $MgSO_4$; digests were pooled for plating on 6 well Primaria plates (Falcon). Cells were cultured until confluent. At confluence, initial plates were collected for RNA isolation and QPCR. Other plates were switched to mineralization medium containing 50 μg/ml ascorbic acid and 10 mM β-glycerophosphate and cultured for an additional 2 weeks, with medium changes every 3–4 days. Bone nodule formation was determined by alizarin red staining of plates after the 2 weeks in culture in mineralization medium.

Immunoblot analysis

Primary osteoblastic cells were isolated as above from neonatal OGR1−/− and wild type mouse calvariae. At confluence, cells were washed in cold PBS, scraped into Laemmli buffer + 100 mM dithiothreitol, boiled for 5 min and stored at −20°C. Parallel cultures were collected in 0.2 N NaOH for determination of protein concentration. Equal amounts of protein were separated on 12% polyacrylamide gels, transferred to Immmobilon-P membranes (Millipore) and immunoblotted with primary antibody to OGR1 (LifeSpan BioSciences) at a 1:1000 dilution, and simultaneously with an actin antibody (Santa Cruz) at a 1:10000 dilution and incubated overnight at 4°C. Specific binding was detected using a secondary antibody coupled to horseradish peroxidase (Vector) and the Clarity Western ECL substrate (BioRad) chemiluminescent detection system for OGR1 and a secondary antibody coupled to dylight 550 (ThermoScientific) for actin. Blots were analyzed on a ChemiDoc MP Imager (BioRad) using a multichannel analyzer.

RNA Isolation and Quantitative Polymerase Chain Reaction

At indicated times, cells were washed with cold PBS and lysed in RLT buffer according to the Qiagen protocol using a Qiashredder. Total RNA was prepared using the Qiagen RNeasy kit(14, 35). RNA (1 μg) was reverse transcribed to first-strand cDNA using an iScript cDNA synthesis kit (Bio-Rad) and specific transcript levels were determined by quantitative real time polymerase chain reaction using iQ SYBR-green in an iCycler thermocycler and analyzed with MyIQ optical system software (Bio-Rad). Primers were synthesized by Integrated DNA Technologies for mouse sequences. Standard curves were generated for each primer. Relative expression levels were normalized to RPL13A RNA levels using the comparative threshold cycle method(36).

Data Analysis

All tests of significance were calculated using analysis of variance, with Bonferroni’s correction for multiple comparisons using conventional computer programs (Statistica, StatSoft).

Acknowledgments

Grant support: National Institutes of Health RO1-AR46289 (to DAB), AR43510 from NIAMS and 1S10RR027340-01 (to BFB) and Renal Research Institute (to NSK, DAB)

The authors acknowledge the technical expertise of Michael Thullen from the Center for Musculoskeletal Research for microCT measurements and Felix Ramos-Busot for immunoblot analyses and thank Dr. Matthew Hilton and Dr. Hani Awad for helpful discussions.

References

1. Lemann J Jr, Bushinsky DA, Hamm LL. Bone buffering of acid and base in humans. Am J Physiol Renal Physiol. 2003; 285:F811–F32. [PubMed: 14532161]
2. Domrongkitchaiporn S, Pongsakul C, Stitchantrakul W, Sirikulchayanonta V, Ongphiphadhanakul B, Radinahamed P, et al. Bone mineral density and histology in distal renal tubular acidosis. Kidney Int. 2001; 59:1086–93. [PubMed: 11231364]

3. Bushinsky, DA. Acidosis and renal bone disease. In: Olgaard, K.; Salusky, IB.; Silver, J., editors. The Spectrum of Mineral and Bone Disorders in Chronic Kidney Disease. New York: Oxford University Press; 2010. p. 253-65.

4. Bushinsky DA, Goldring JM, Coe FL. Cellular contribution to pH-mediated calcium flux in neonatal mouse calvariae. Am J Physiol (Renal Fluid Electrolyte Physiol 17). 1985; 248:F785–F9.

5. Bushinsky DA, Sessler NE, Glena RE, Featherstone JDB. Proton-induced physicochemical calcium release from ceramic apatite disks. J Bone Miner Res. 1994; 9:213–20. [PubMed: 8140934]

6. Krieger NS, Frick KK, Bushinsky DA. Mechanism of acid-induced bone resorption. Current Opin in Nephrol Hypertens. 2004; 13:423–36.

7. Bushinsky DA. Net calcium efflux from live bone during chronic metabolic, but not respiratory, acidosis. Am J Physiol (Renal Fluid Electrolyte Physiol 25). 1989; 256:F836–F42.

8. Krieger NS, Sessler NE, Bushinsky DA. Acidosis inhibits osteoblastic and stimulates osteoclastic activity in vitro. Am J Physiol (Renal Fluid Electrolyte Physiol 31). 1992; 262:F442–F8.

9. Frick KK, Bushinsky DA. Chronic metabolic acidosis reversibly inhibits extracellular matrix gene expression in mouse osteoblasts. Am J Physiol (Renal Physiol 44). 1998; 275:F840–F7.

10. Frick KK, Jiang L, Bushinsky DA. Acute metabolic acidosis inhibits the induction of osteoblastic egr-1 and type 1 collagen. Am J Physiol (Cell Physiol 41). 1997; 272:C1450–C6.

11. Sprague SM, Krieger NS, Bushinsky DA. Greater inhibition of in vitro bone mineralization with metabolic than respiratory acidosis. Kidney International. 1994; 46:1199–206. [PubMed: 7861717]

12. Krieger NS, Parker WR, Alexander KM, Bushinsky DA. Prostaglandins regulate acid-induced cell-mediated bone resorption. Am J Physiol Renal Physiol. 2000; 279:F1077–F82. [PubMed: 11097626]

13. Krieger NS, Frick KK, LaPlante Strutz K, Michalenka A, Bushinsky DA. Regulation of COX-2 mediates acid-induced bone calcium efflux in vitro. Journal of Bone and Mineral Research. 2007; 22(6):907–17. [PubMed: 17352658]

14. Frick KK, Bushinsky DA. Metabolic acidosis stimulates RANK ligand RNA expression in bone through a cyclooxygenase dependent mechanism. Journal of bone and mineral research. 2003; 18:1317–25. [PubMed: 12854843]

15. Boyce BF, Xing L. Functions of RANKL/RANK/OPG in bone modeling and remodeling. Archives of Biochemistry and Biophysics. 2008; 473(2):139–46. [PubMed: 18395508]

16. Frick KK, Krieger NS, Nehrke K, Bushinsky DA. Metabolic acidosis increases intracellular calcium in bone cells through activation of the proton receptor OGR1. Journal of bone and mineral research. 2009; 24(2):305–13. [PubMed: 18847331]

17. Ludwig MG, Vanek M, Gueirine D, Gasser JA, Jones CE, Junker U, et al. Proton-sensing G-protein-coupled receptors. Nature. 2003; 425:93–8. [PubMed: 12955148]

18. Tomura H, Wang JQ, Liu Jp, Komachi M, Damirin A, Mogi C, et al. Cyclooxygenase-2 expression and prostaglandin E 2 production in response to acidic pH through OGR1 in a human osteoblastic cell line. Journal of Bone and Mineral Research. 2008; 23(0):1129–39. [PubMed: 18302504]

19. Tomura H, Mogi C, Sato K, Okajima F. Proton-sensing and lysolipid-sensitive G-protein-coupled receptors: A novel type of multi-functional receptors. Cellular Signalling. 2005; 17(12):1466–76. [PubMed: 16014326]

20. Krieger NS, Bushinsky DA. Pharmacologic inhibition of intracellular calcium release blocks acid-induced bone resorption. Am J Physiol Renal Physiol. 2011; 300:F91–7. [PubMed: 21048027]

21. Singer D. Metabolic adaptation to hypoxia: cost and benefit of being small. Respiratory Physiology & Neurobiology. 2004; 141(3):215–28. [PubMed: 15288595]

22. Bushinsky DA, Frick KK. The effects of acid on bone. Current Opinion in Nephrology and Hypertension. 2000; 9:369–79. [PubMed: 10926173]

23. Krieger NS, Bushinsky DA, Frick KK. Cellular mechanisms of bone resorption induced by metabolic acidosis. Semin Dial. 2003; 16:463–6. [PubMed: 14629607]

24. Seuwen K, Ludwig MG, Wolf RM. Receptors for protons or lipid messengers or both? Journal of Receptors and Signal Transduction. 2006; 26(5–6):599–610. [PubMed: 17118800]

25. Kobayashi Y, Udagawa N, Takahashi N. Action of RANKL and OPG for osteoclastogenesis. Crit Rev Eukaryot Gene Expr. 2009; 19(1):61–72. [PubMed: 19191757]

26. Komarova SV, Pereverzev A, Shum JW, Sims SM, Dixon SJ. Convergent signaling by acidosis and receptor activator of NF-kB ligand (RANKL) on the calcium/calcineurin/NFAT pathway in osteoclasts. Proceedings of the National Academy of Sciences. 2005; 102(7):2643–8.

27. Yang M, Mailhot G, Birnbaum MJ, MacKay CA, Mason-Savas A, Odgren PR. Expression of and role for ovarian cancer G-protein-coupled receptor 1 (OGR1) during osteoclastogenesis. Journal of Biological Chemistry. 2006; 281(33):23598–605. [PubMed: 16787916]

28. Pereverzev A, Komarova SV, Korcok J, Armstrong S, Tremblay GB, Dixon SJ, et al. Extracellular acidification enhances osteoclast survival through an NFAT-independent, protein kinase C-dependent pathway. Bone. 2008; 42(1):150–61. [PubMed: 17964236]

29. Li H, Wang D, Singh LS, Berk M, Tan H, Zhao Z, et al. Abnormalities in osteoclastogenesis and decreased tumorigenesis in mice deficient for ovarian cancer G protein-coupled receptor 1. PLoS ONE. 2009; 4(5):e5705. [PubMed: 19479052]

30. Silva BC, Bilezikian JP. Parathyroid hormone: anabolic and catabolic actions on the skeleton. Current Opinion in Pharmacology. 2015; 22:41–50. [PubMed: 25854704]

31. Tomura H, Wang JQ, Komachi M, Damirin A, Mogi C, Tobo M, et al. Prostaglandin I_2 production and cAMP accumulation in response to acidic extracellular pH through OGR1 in human aortic smooth muscle cells. Journal of Biological Chemistry. 2005; 280(41):34458–64. [PubMed: 16087674]

32. Singh LS, Berk M, Oates R, Zhao Z, Tan H, Jiang Y, et al. Ovarian cancer G protein–coupled receptor 1, a new metastasis suppressor gene in prostate cancer. Journal of the National Cancer Institute. 2007; 99(17):1313–27. [PubMed: 17728215]

33. Sun X, Yang LV, Tiegs BC, Arend LJ, McGraw DW, Penn RB, et al. Deletion of the pH sensor GPR4 decreases renal acid excretion. Journal of the American Society of Nephrology. 2010; 21(10):1745–55. [PubMed: 20798260]

34. Krieger NS, Hefley TJ. Differential effects of parathyroid hormone on protein phosphorylation in two osteoblast-like cell populations isolated from neonatal mouse calvaria. Calc Tiss Int. 1989; 44:192–9.

35. Krieger NS, Culbertson CD, Kyker-Snowman K, Bushinsky DA. Metabolic acidosis increases fibroblast growth factor 23 in neonatal mouse bone. American Journal of Physiology - Renal Physiology. 2012; 303:F431–6. [PubMed: 22647635]

36. Livak KJ, Schmittgen TD. Analysis of relative gene expression data using real-time quantitative PCR and the 2−[Delta][Delta]CT method. Methods. 2001; 25(4):402–8. [PubMed: 11846609]

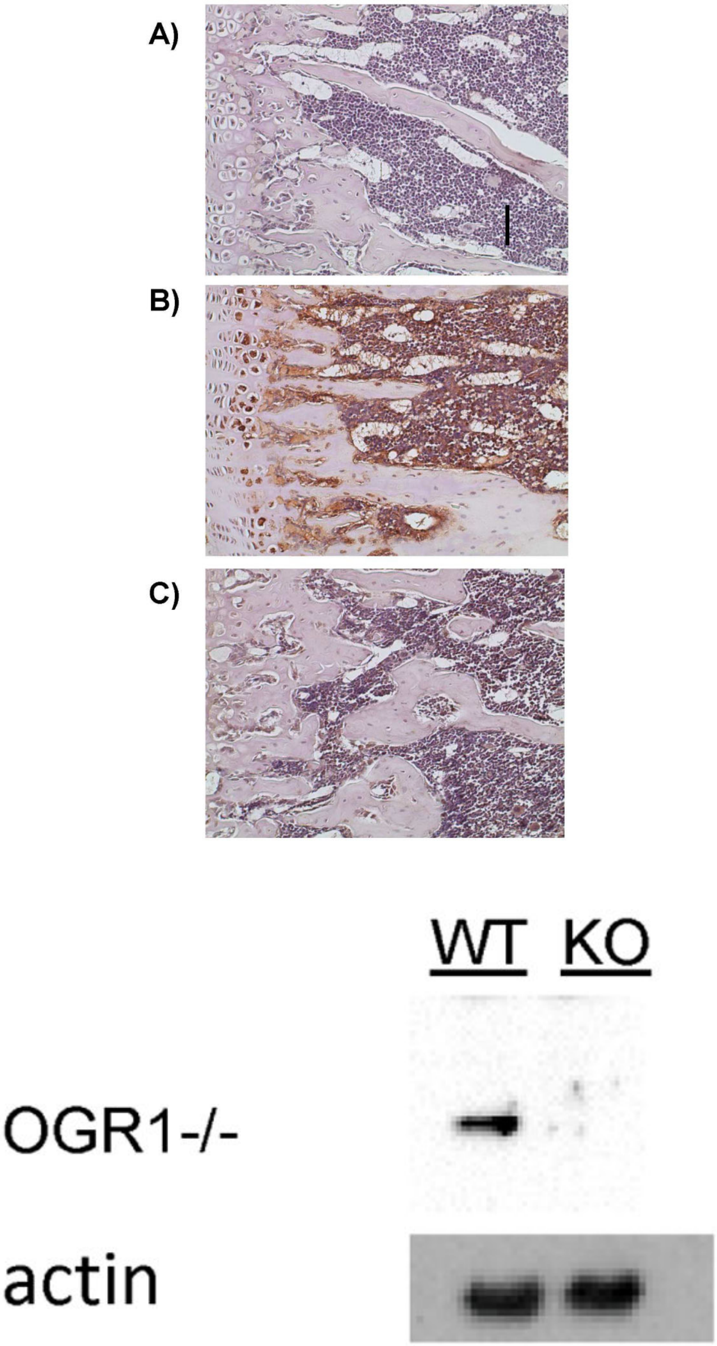

Figure 1. OGR1 staining was not detectable by immunohistochemical analysis in tibial sections from 8 week OGR1−/− mice compared to wild type (WT) sections

A) WT decalcified tibial section incubated with no primary antibody; B) WT decalcified tibial section incubated with specific primary antibody to OGR1; C) OGR1−/− decalcified tibial section incubated with specific primary antibody to OGR1. 20x magnification, scale bar = 100 μm. D) Immunoblot of total protein from osteoblast lysates detects OGR1 from WT but not OGR1−/− primary osteoblasts. Data are normalized to actin.

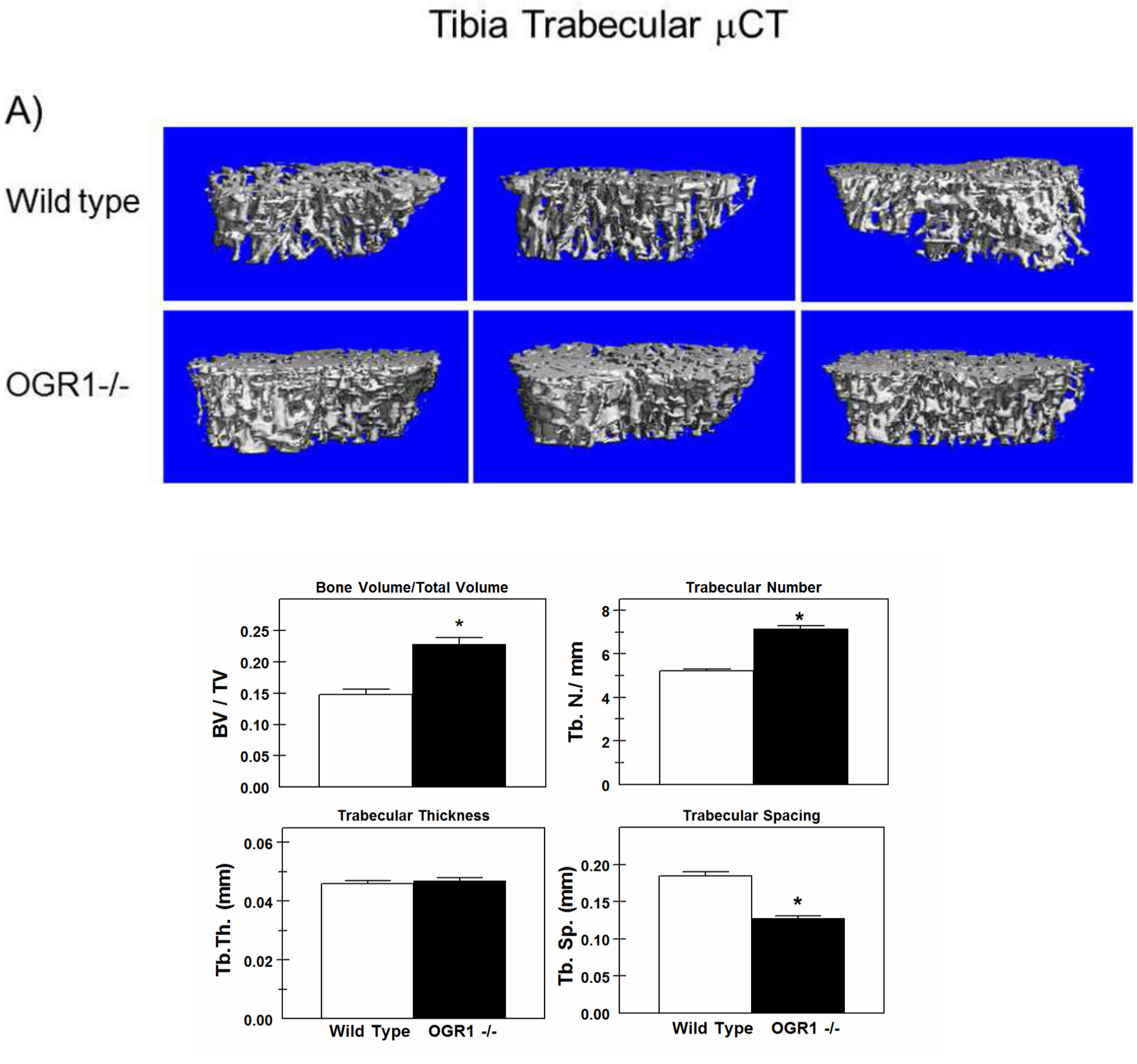

Figure 2. MicroCT analysis of tibial metaphyseal trabecular bone from 8 week old male wild type and OGR1−/− mice

A) Representative μCT scans of wild type (upper panels) and OGR1−/− tibiae (lower panels). B) Quantitative analysis of μCT scans: Bone Volume/Total Volume (BV/TV), Trabecular Number (Tb.N.), Trabecular Thickness (Tb.Th.) and Trabecular Spacing (Tb.Sp.); mean ± SE for 12 wild type and 11 OGR1−/− mice. *, $p<0.05$ vs wild type bone.

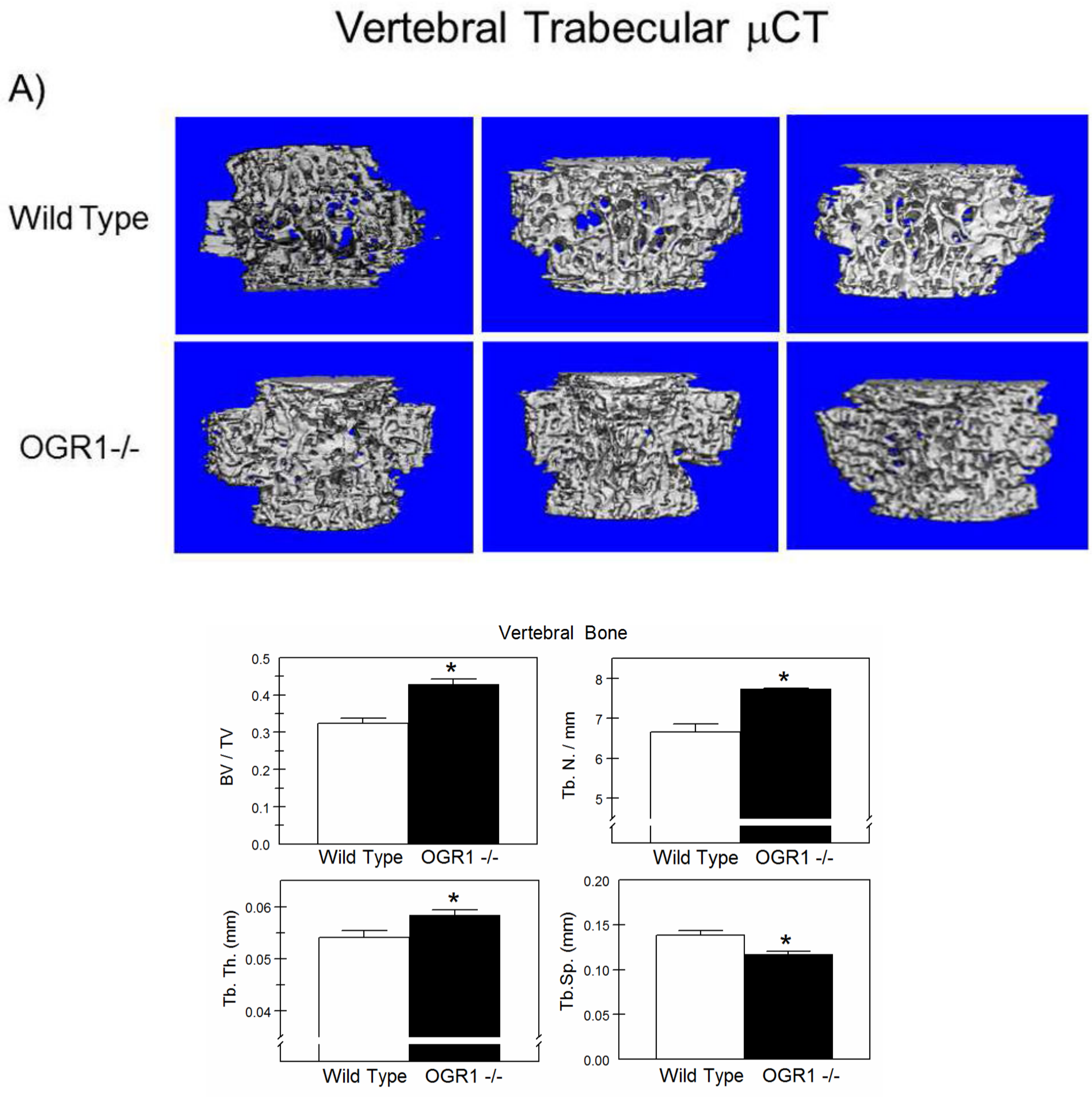

Figure 3. MicroCT analysis of vertebral trabecular bone from 8 week-old male wild type and OGR1−/− mice

A) Representative μCT scans of vertebrae from wild type (upper panels) and OGR1−/− (lower panels) mice. B) Quantitative analysis of μCT scans: Bone volume/total volume (BV/TV), Trabecular Number (Tb.N.), Trabecular Thickness (Tb.Th.) and Trabecular Spacing (Tb.Sp.); mean ± SE for 12 wild type and 11 OGR1−/− mice. *, $p<0.05$ vs wild type bone.

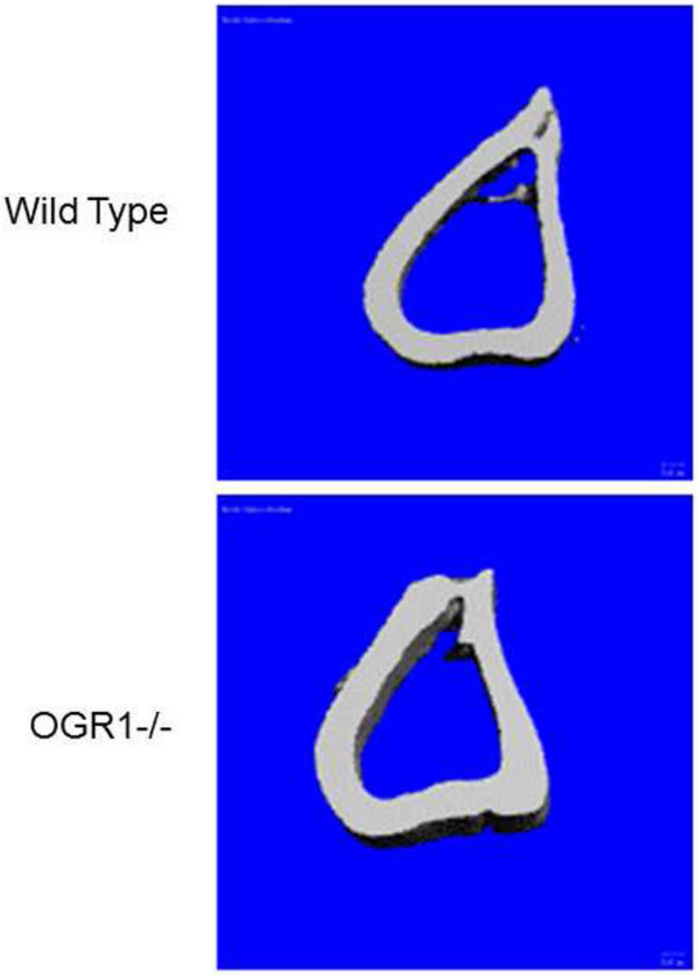
Wild Type
OGR1-/-

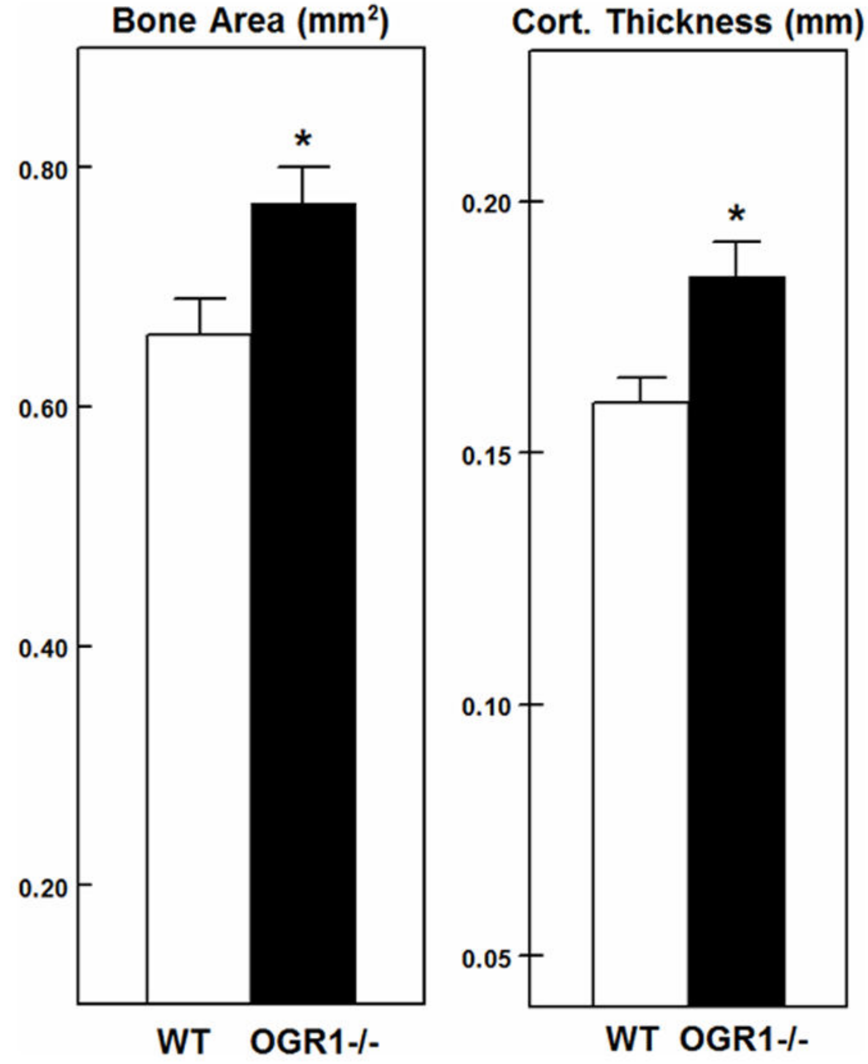

Figure 4. MicroCT analysis of tibia cortical bone volume from 8 week old male wild type and OGR1−/− mice

A) Representative μCT scans of wild type tibia (upper panel) and OGR1−/− tibia (lower panel). B) Quantitative analysis of cortical bone area (on left) and cortical thickness (on right) for wild type (open bars) and OGR1−/− (solid bars). Results are mean ± SE for 10 wild type and 6 OGR1−/− mice; *, $p<0.05$ vs wild type bone.

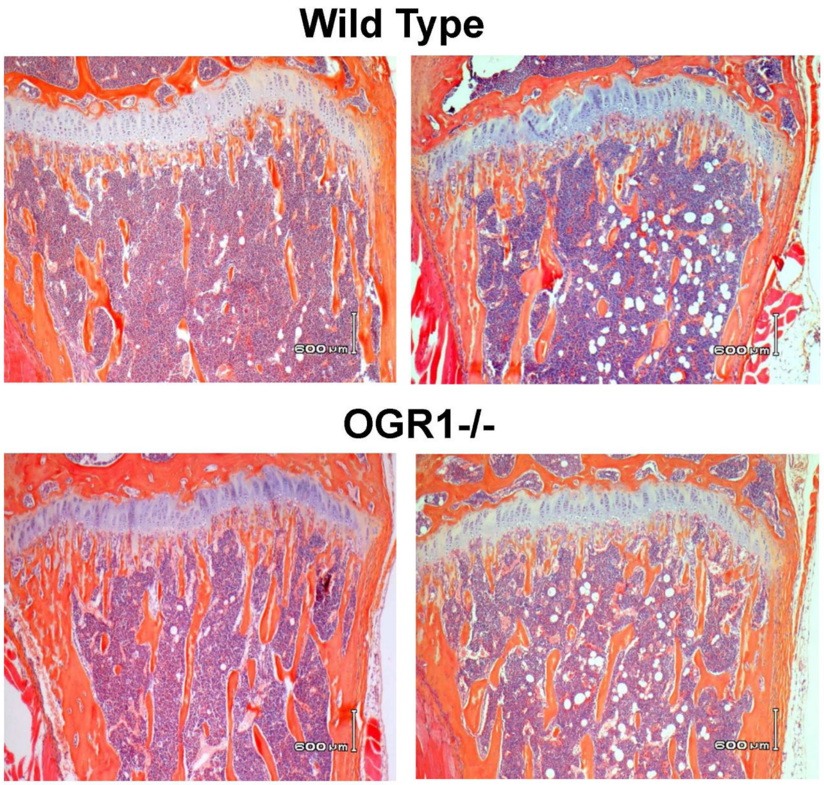
Wild Type
600 µm
600 µm
OGR1-/-
600 µm
600 µm

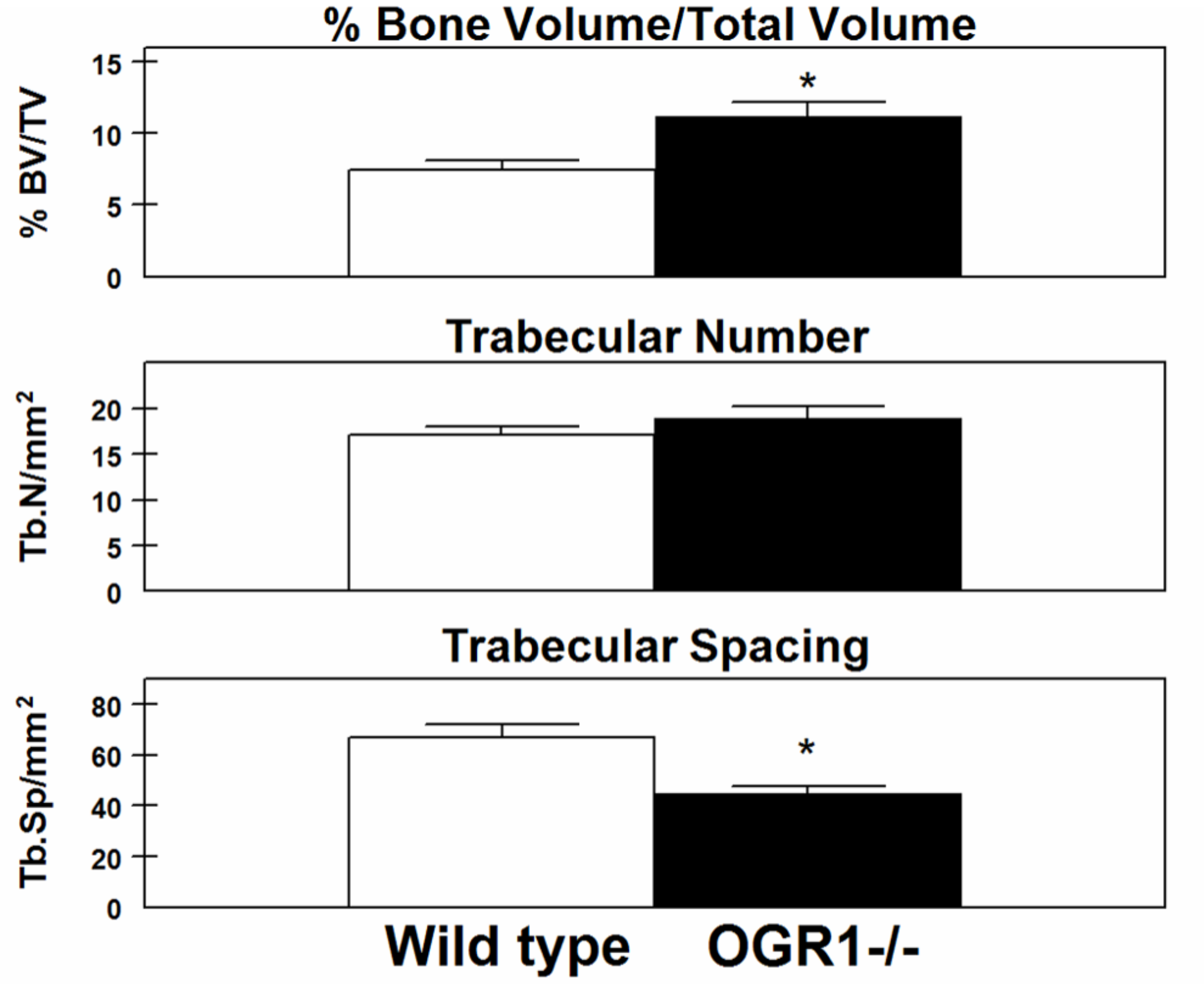

Figure 5. Increased trabecular bone volume in the tibial metaphysis from 8 week-old OGR1−/− mice compared to wild type mice

A) Representative tibial sections were stained with H&E and orange G, which displays trabecular bone in orange, from wild type (upper panels) and OGR1−/− (lower panels) mice. B) Quantitative histomorphometric analysis of trabecular bone from undecalcified tibial sections of wild type (open bars) and OGR1−/− (solid bars) mice using Visiopharm software: Bone Volume/Total Volume (BV/TV), Trabecular Number (Tb.N), Trabecular Spacing (Tb. Sp). Results are mean ± SE for 9 wild type and 7 OGR1−/− mice; *, $p<.05$ vs wild type bone.

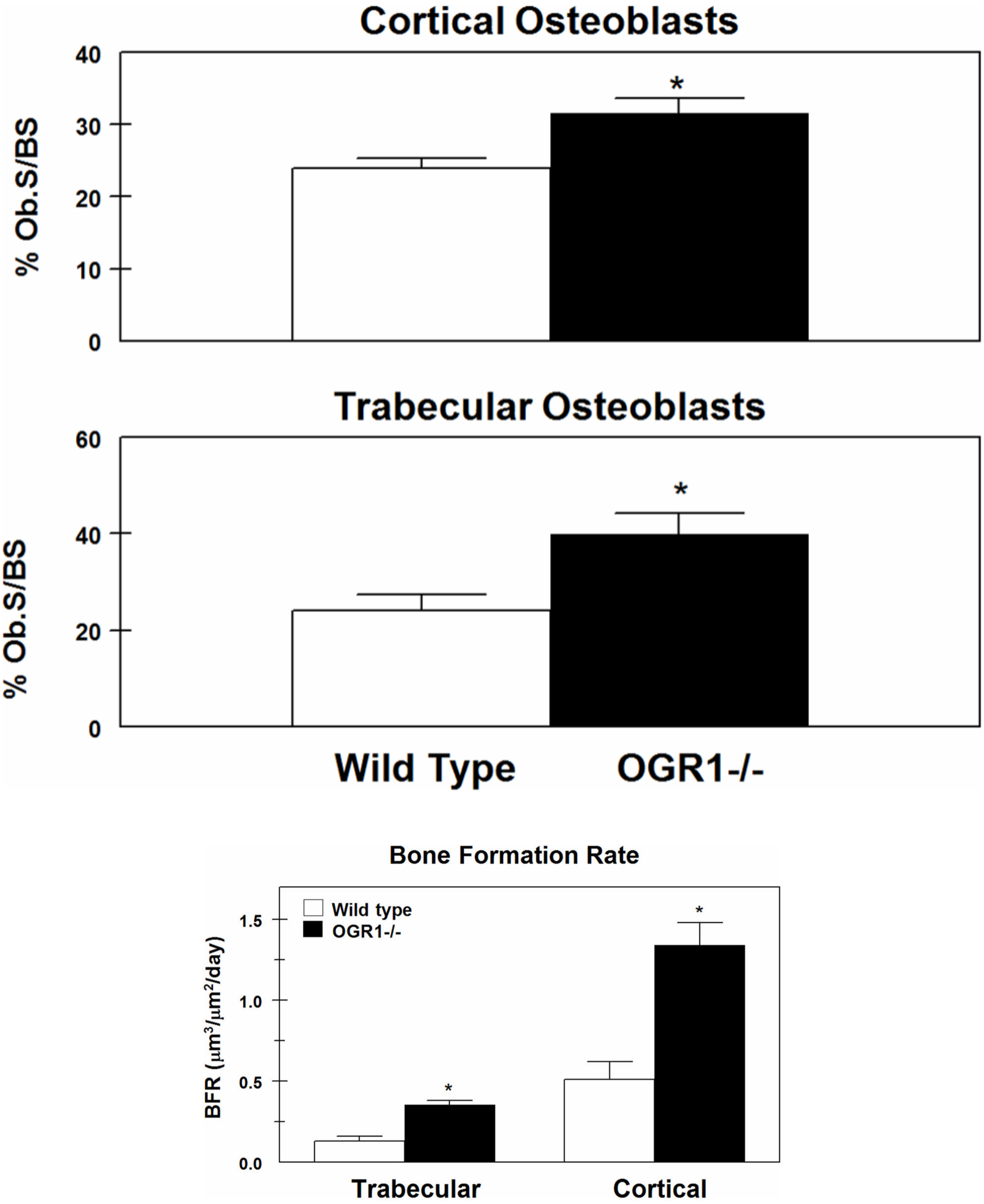

Figure 6. Histomorphometric analysis of osteoblast number from tibial endocortical bone surfaces of 8 week-old wild type and OGR1−/− mice

A) Quantitative analysis of osteoblasts along the endocortical bone (upper panel) and trabecular (lower panel) surface of sections from wild type (open bars) and OGR1−/− (solid bars) using OsteoMeasure software for endocortical measurements and Visiopharm software for trabecular measurements, normalized to bone surface. Results are mean ± SE for 7 wild type and 6 OGR1−/− mice; *, $p<0.05$ vs wild type. B) Bone formation rates in tibiae from 8 week-old wild type or OGR1−/− mice. Mice were injected with calcein 14 days and again 2 days prior to sacrifice. Bones were fixed, embedded in plastic and sectioned. Quantitative analyses of bone formation rates were determined from analysis of the resultant fluorescent images: sections of wild type (open bars) and OGR1−/− (solid bars) tibiae; trabecular (left) and endocortical (right) bone. Results are mean ± SE for 6 for wild type and 4 for OGR1−/− mice; *, $p<.05$ vs wild type.

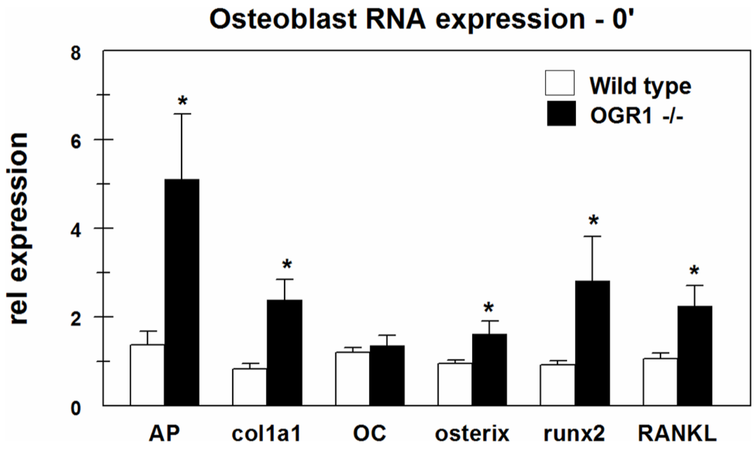
Osteoblast RNA expression - 0'
rel expression
0
2
4
6
8
Wild type
OGR1 -/-
*
*
*
*
*
AP
col1a1
OC
osterix
runx2
RANKL

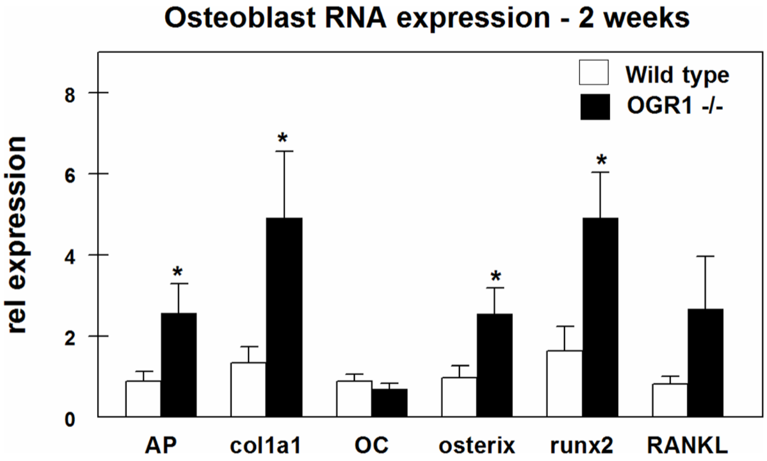
Osteoblast RNA expression - 2 weeks
rel expression
0
2
4
6
8
Wild type
OGR1 -/-
*
*
*
*
AP
col1a1
OC
osterix
runx2
RANKL

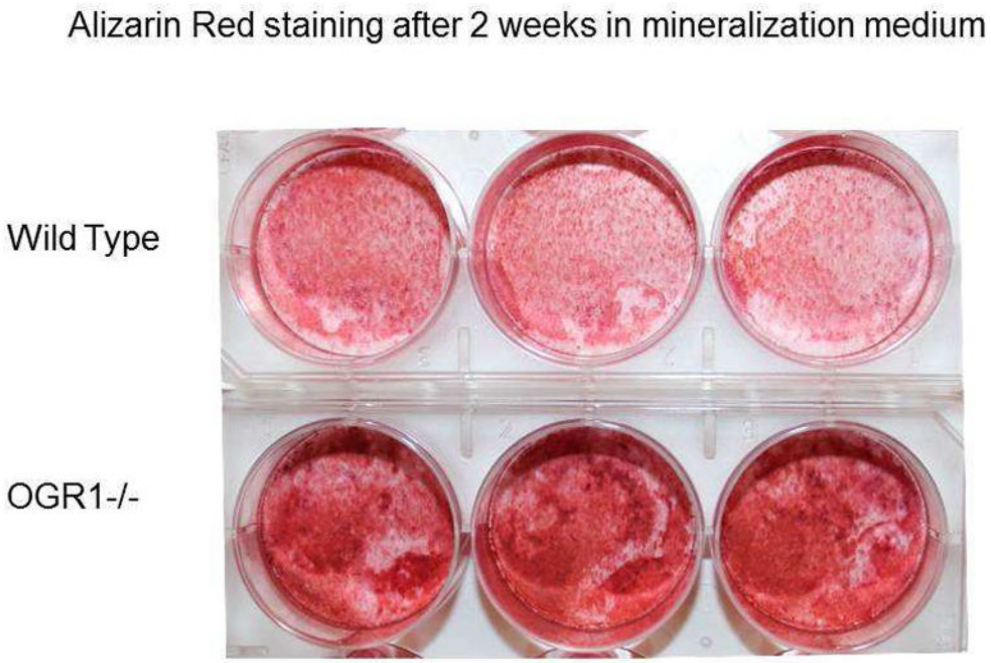
Alizarin Red staining after 2 weeks in mineralization medium
Wild Type
OGR1-/-

Figure 7. Osteoblastic gene expression in primary cells from wild type and OGR1−/− neonatal calvariae

A) Primary calvarial osteoblasts were grown to confluence and total RNA isolated. Relative expression of alkaline phosphatase (AP), collagen 1a1 (col1a1), osteocalcin (OC), osterix, runx2 and RANKL were analyzed by QPCR relative to the housekeeping gene RPL13a. B) Additional confluent cultures were switched to mineralization medium for an additional 2 weeks, at which time, total RNA was isolated and analyzed for expression of the same osteoblastic genes following this additional differentiation. Results are the mean ± SE for 26–30 replicate cultures in each group. *p<0.05 compared to wild type expression of the indicated gene. C) Increased alizarin red staining of OGR1−/− compared to wild type primary osteoblasts after 2 weeks in mineralization medium.

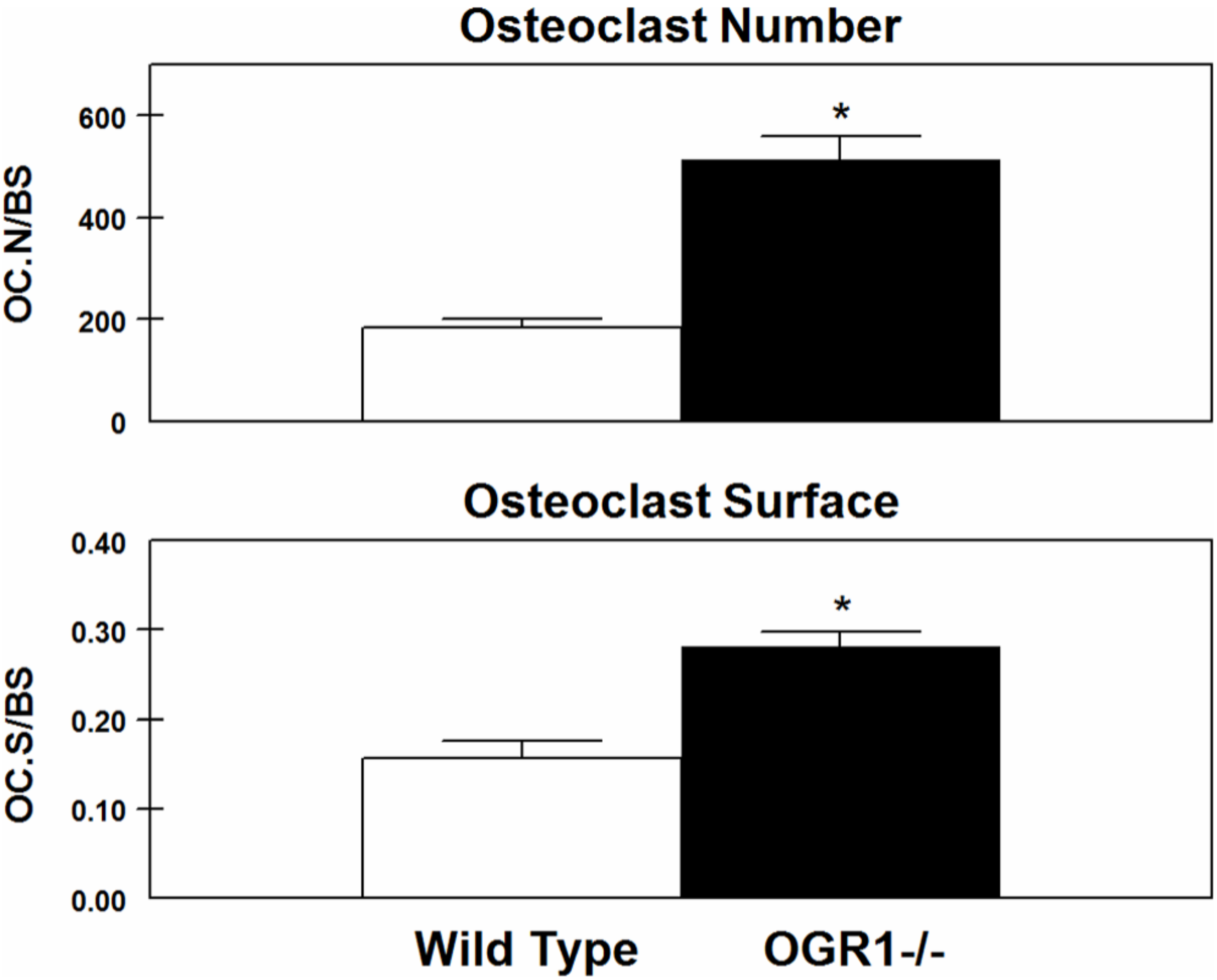
Osteoclast Number
OC.N/BS
0
200
400
600
*
Osteoclast Surface
OC.S/BS
0.00
0.10
0.20
0.30
0.40
*
Wild Type
OGR1-/-

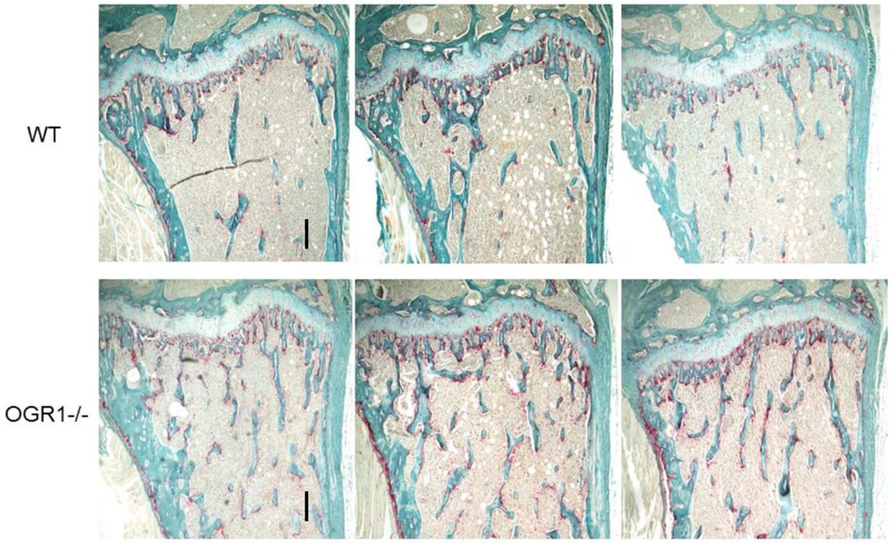

Figure 8. Increased osteoclasts in the tibial metaphyses of 8 week-old OGR1−/−mice compared to wild type mice

A) Quantitative histomorphometric analysis of osteoclast number and surface area from tibiae from wild type (open bars) and OGR1−/− (solid bars) mice using Visiopharm software. Results are mean ± SE for 9 wild type and 7 OGR1−/− mice; *, $p<.05$ vs wild type bone. B) Detection of tartrate resistant acid phosphatase (TRAP) staining of osteoclasts in tibiae from 8 week-old wild type and OGR1−/− mice. Tibial sections were stained for tartrate resistant acid phosphatase activity, which is observed as red staining. Representative images of wild type (upper panels) and OGR1−/− (lower panels) tibial sections (5x magnification, scale bar = 600 μm).